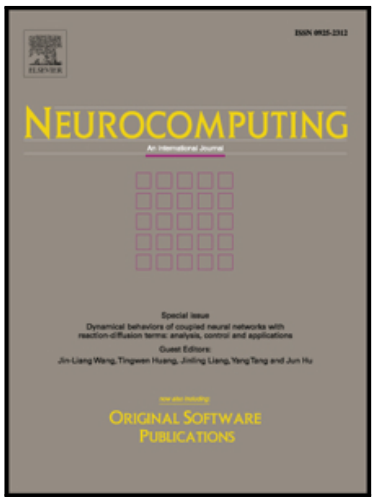

Recognizing tactile surface roughness with a biomimetic fingertip: a soft neuromorphic approach

Yi Zhengkun , Zhang Yilei

PII: S0925-2312(17)30520-9
DOI: 10.1016/j.neucom.2017.03.025
Reference: NEUCOM 18246

To appear in: *Neurocomputing*

Received date: 8 October 2016
Revised date: 6 January 2017
Accepted date: 11 March 2017

Please cite this article as: Yi Zhengkun , Zhang Yilei , Recognizing tactile surface roughness with a biomimetic fingertip: a soft neuromorphic approach, *Neurocomputing* (2017), doi: 10.1016/j.neucom.2017.03.025

Recognizing tactile surface roughness with a biomimetic fingertip: a soft neuromorphic approach

Yi Zhengkun, Zhang Yilei
School of Mechanical and Aerospace Engineering, Nanyang Technological University, 50 Nanyang Avenue, Singapore 639798

E-mail: ylzhang@ntu.edu.sg

Abstract: Surface roughness is an important object property and can significantly affect the friction characteristics, wear resistance, and fatigue life of components. Although some work has been done on demonstrating the capability of specific tactile sensors for surface roughness discrimination, the soft neuromorphic approach by taking inspirations from neuroscience for tactile surface roughness discrimination is exceptionally rare. This paper aims to fill this gap, and presents a soft neuromorphic method for tactile surface roughness discrimination with a biomimetic fingertip. The analog tactile signals generated from polyvinylidene difluoride (PVDF) films are fed as input to the Izhikevich neurons in order to obtain spike trains. Two distinct decoding schemes based on *k*-nearest neighbors (*k*NN) in both spike feature space and spike train space are used for surface roughness discrimination. We thoroughly examined the different spike train distance based *k*NN (STD-*k*NN) algorithms for decoding spike trains. Eight standard rough surfaces with roughness values (Ra) of 50 μm, 25 μm, 12.5 μm, 6.3 μm 3.2 μm, 1.6 μm, 0.8 μm, and 0.4 μm are explored. The highest classification accuracy of (77.6 ± 13.7) % can be achieved with *k*NN (k = 11) classifier and the Victor-Purpura distance ($q = 0.024\ \mathrm{ms}^{-1}$).

Keywords: soft neuromorphic approach; spike train distance; biomimetic fingertip; tactile sensing; surface roughness recognition

1. Introduction

Neuromorphic engineering is an interdisciplinary domain that takes inspirations from neuroscience. It aims to mimic the neuronal architectures and function of nervous systems by the aid of electronic devices [1]. The past decade has witnessed tremendous efforts and progress made by the industry and academia with many neuromorphic designs and hardware developments. For instance, the address event representation (AER) is used as a signal transmission scheme in recent neuromorphic systems, which addresses the connectivity challenge of a large number of neurons on a silicon chip [2]. Neuromorphic scientists have also developed silicon retinas and silicon cochleas to replicate the functionality of retina and cochlea [3,4]. These systems have been demonstrated to possess biological properties such as local processing and local gain control. In addition to the surge in hardware development, there is another branch of neuromorphic engineering called soft neuromorphic engineering [5], which focuses on spike-

like signal processing, mainly on spiking neural networks. External stimuli in most sensory systems are encoded, processed and transmitted as action potentials namely, spikes [6]. Even though that the transformation from the external information to spikes could impose penalties such as the loss of information and reduction in signal entropy [7,8], it has many advantages, for instance, spikes are immune to attenuation during propagation over long distances [9], and possess a good anti-noise capability [10].

Recently, soft neuromorphic engineering has been employed in several tactile sensing applications such as gait event detection [11] and Braille letter recognition [12]. However, a soft neuromorphic approach for tactile surface roughness discrimination is exceptionally rare. As a major component of surface texture apart from other characteristics such as waviness and lay, surface roughness is an important object property and can significantly affect the friction characteristics, wear resistance, and fatigue life of components [13]. Therefore, this paper aims to fill this gap by investigating a soft neuromorphic method for tactile surface roughness discrimination. Another motivation of this paper originates from bionic engineering, for example, prosthetic limbs [14]. In an able-bodied human, tactile stimuli like force and vibration can be detected by the mechanoreceptors embedded in the skin, and will be conveyed to the specific target in the brain or spinal cord. However, the outputs of artificial tactile sensors in a sensorized neural prosthesis are usually continuous and need to be processed before delivered to the tactile afferents. Therefore, the study of prosthetics with spike-like signals may provide new insight into the development of advanced neuroprostheses.

This paper focuses on two areas: (1) surface roughness encoding with spiking neuron models using a biomimetic fingertip; (2) interpretation of spike trains with distinct decoding schemes based on *k*-nearest neighbors (*k*NN) in both spike feature space and spike train space. Figure 1 illustrates the soft neuromorphic method for tactile surface roughness discrimination using a biomimetic fingertip in this paper. The paper is organized as follows: following the Introduction, the related previous work and contribution are described in Section 2 and Section 3, respectively. Subsequently, we give a detailed description of the materials and methods for tactile surface roughness discrimination in Section 4. We then present the results and discussion in Section 5 followed by the conclusion in Section 6.

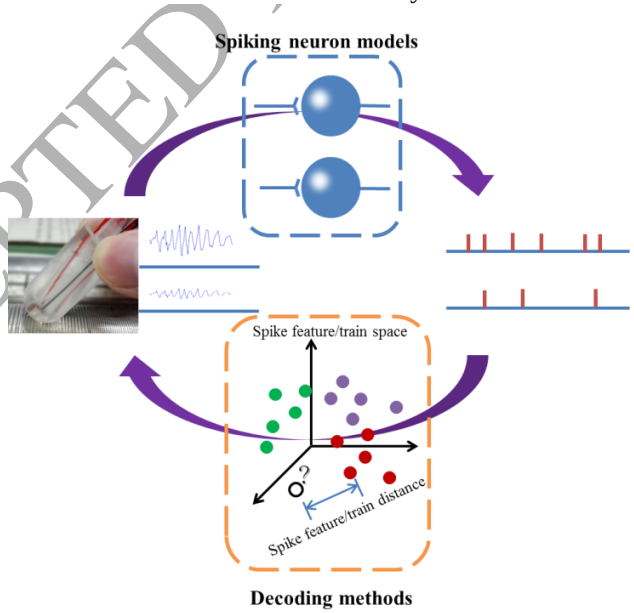

Figure 1. Soft neuromorphic method for tactile surface discrimination using a biomimetic fingertip. The analog signals generated by tactile sensors are converted into spikes via spike neuron models. The spike train decoding schemes are based on *k*-nearest neighbors (*k*NN) in both spike feature space and spike train

space.

2. Related work

2.1. Neurophysiology of roughness perception

Human beings possess the capability to sensitively perceive different materials [15], but the question remains as to how human beings encode the surface roughness during the physical finger-surface interactions. Extensive researches have been conducted to investigate the mechanisms underlying the perceived surface roughness [16–18]. Connor et al. [17], proposed that the neural coding of tactile texture is closely related to the spatial variations in slowly adapting (SA) mechanoreceptive afferents, which was limited to the coarse surfaces with element spaces of $>$ 1mm. Yoshioka et al. [18] extended Connor et al.'s work by studying the neural coding mechanisms for the roughness perception of the finely textured surface, and found that there is a consistent relationship between human judgements of fine surface roughness and slowly adapting type I (SA-I) spatial variations. However, a recent study showed that the tactile roughness discrimination relies mainly on vibration sensitive afferents [16]. The fast adapting type I (FA-I) mechanoreceptors (Meissner's corpuscles) and the fast adapting type II (FA-II) mechanoreceptors (Pacinian corpuscles) are generally regarded to be responsible for modulating the vibratory stimuli occurring at the interface of explored surfaces and the fingers.

2.2. Surface roughness classification using artificial tactile sensors

Tremendous efforts have been made to recognize the surface texture using artificial tactile sensors or artificial fingers [19–22]. However, relatively few investigations have been conducted to discriminate surface roughness. Oddo et al. [23], fabricated a 2×2 tactile piezoresistive sensor array based on microfabrication technology, which was embedded in a polymeric packaging with fingerprint-like structures. The density of the tactile sensing elements was considered to be equivalent to that of human slow adapting type I (SA-I) mechanoreceptors. Three gratings with 400 μm, 440 μm and 480 μm spatial periods were explored. The wavelet and cross-wavelet transforms were performed to extract tactile features, and a classification accuracy of 97.6% was achieved by a *k*-Nearest Neighbors (*k*NN) classifier. Peiner et al. [24], developed a tactile cantilever sensor intended for high-aspect-ratio micrometrology with a resolution of 10-20 nm when scanning at a velocity of 0.63 mm/s. However, this sensor was prone to wear or damage. Muhammad et al. [20], developed a capacitive tactile sensor array to recognize fabrics with groove width varied from 200 μm to 1000 μm in increments of 200 μm. The surface roughness discrimination was performed by assessing the peak frequency of frequency spectrum generated by capacitive sensors.

2.3. Soft neuromorphic methods for tactile sensing

Tactile sensing by the aid of neuromorphic engineering has attracted increasing attention in the past decade. Lee et al. [25], used a fabric based binary tactile sensor array to discriminate local curvature of objects. The tactile signals were converted into spikes using two Izhikevich models. Subsequently, a tempotron classifier [26] was employed to distinguish between the 105 mm indenter and 65 mm indenter based on the relative timings of first spikes. Lee et al. [11], also applied the soft neuromorphic method for gait event detection using a low-cost, foot pressure sensor. The decoding scheme employed in this work is the synaptic kernel inverse method (SKIM) instead of the tempotron classifier. Bologna et al. [12] used a 4×6 capacitive square sensor array to recognize the Braille letters. In contrast to Lee et al.'s work, their work was distinct in both analog-to-spike transformation model and pattern decoding algorithms. Specifically, the transformation was implemented by integrate-and-fire models, and a naïve Bayesian classifier was trained to perform online Braille letter recognition. A more closely related work on naturalistic texture categorization was reported by Rongala et al. [27], where they also performed the

analog-to-spike transformation using the Izhikevich models, and implemented two decoding procedures. One was based on spike feature including the average spike rate and the coefficient of variance of the interspike intervals. The other was based on precise spike timing by the aid of the Victor-Purpura distance. One work on surface roughness discrimination in a soft neuromorphic fashion was reported by Spigler et al. [5], where they presented a grating recognition system by incorporating the Izhikevich model and stimulus decoding scheme via assessing the principal frequency in the spike frequency domain. Table 1 summarizes the relevant papers of tactile sensing using soft neuromorphic methods.

Table 1. Tactile sensing using soft neuromorphic methods.

Year	Author	Tactile Sensor	Analog-to-spike Transformation	Spike Train Decoding	Application
2012	Spigler et al. [5]	A 2×2 piezoresistive tactile sensor array	The Izhikevich model	Spike frequency domain analysis	Grating discrimination
2013	Bologna et al. [12]	A 4×6 capacitive square tactile sensor array	The integrate-and-fire model	Naïve Bayesian classifier	Braille letter recognition
2013	Lee et al. [25]	A fabric based binary tactile sensor array	The Izhikevich model	Tempotron	Curvature discrimination
2014	Lee et al. [11]	A low-cost, foot pressure sensor	The Izhikevich model	The synaptic kernel inverse method (SKIM)	Gait event detection
2015	Rongala et al. [27]	A 2×2 piezoresistive tactile sensor array	The Izhikevich model	Scheme 1: *k*-nearest neighbors based on spike features Scheme 2: *k*-nearest neighbors based on the Victor-Purpura Distance	Texture Discrimination

3. Contribution

The main contributions of this paper include the following: (1) we present a soft neuromorphic method for tactile surface roughness discrimination using a biomimetic fingertip, (2) we set out a straightforward examination of different spike train distance based on *k*-nearest neighbors (STD-*k*NN) algorithms in spike train space for tactile surface roughness discrimination.

Comparing with the previous work [23,27], which mimicked only SA-I mechanoreceptors (Merkel mechanoreceptors), our work is inspired by the surface roughness perception ability of Meissner's corpuscles (FA-I mechanoreceptors). Compared to Rongala et al.'s work [27] that only investigated the Victor-Purpura distance, this paper thoroughly examines various spike train distances including both parameter-dependent and parameter-free distances based on *k*NN. In addition, any other spike train distance could be easily employed in the unified framework of the STD-*k*NN. This paper is also different from Rongala et al.'s work [27] by focusing on the recognition of surface roughness, which is a major component of texture, but has rarely been explored. Compared to the previous work in tactile surface roughness discrimination using a neuromorphic approach [5], our work is different in terms of decoding algorithms and test surfaces to be explored. The problem in this paper is formulated as a multi-class classification problem instead of binary classification problem, where multiple and complex surface samples are explored.

4. Materials and methods

4.1. Biomimetic fingertip

(a) Biomimetic fingertip (b) Biomimetic versus human fingertip

Figure 2. (a) Biomimetic artificial fingertip, and (b) biomimetic vs. human fingertip. The structures of both human and biomimetic fingertips contain two layers with different hardness, and a bone.

The biomimetic fingertip used in the experiment is shown in Figure 2. The structure of our designed artificial fingertip resembles that of a human fingertip, which is comprised of epidermis, dermis, and a bone. The skin of human beings [28] is inherently elastic and consists of two layers, i.e., the epidermis and dermis. The hardness of the epidermis is higher than that of the dermis. In this paper, we mimic skin's elastic properties using polydimethylsiloxane (PDMS) elastomer. The hardness difference between epidermis and dermis is emulated by altering the base to curing agent mixing ratio. A polymethyl methacrylate (PMMA) bar serves the role comparable to that of a bone. In addition, the similar locations of Meissner's corpuscles, which lie just beneath the epidermis [29], are replicated by embedding the polyvinylidene difluoride (PVDF) films between the two PDMS layers. PVDF film is a classic example of piezoelectric polymers that is widely used as tactile sensors [30–33], and exhibit a very good high-frequency response, which makes them extremely suitable for measuring vibrations. In our previous work, the capability of a PVDF film sensor to mimic tactile FA-I afferent has been successfully demonstrated by employing spiking neuron models and the model outputs agree reasonably well with biological measurements under the vibratory stimuli [34].

4.2. Spiking neuron models

Spiking neuron models [35] provide a bridge between analog signals and spike trains, and they are able to convert the analog signals into spike trains. There are many spiking neuron models proposed by neuroscientists, such as the Hodgkin-Huxley model [36] and the integrate-and-fire model [37]. The Hodgkin-Huxley model is rather complicated which is described by four coupled nonlinear differential equations. It is demonstrated to be biophysically accurate. However, the Hodgkin-Huxley model is computationally prohibitive and difficult to analyze mathematically. On the contrary, the integrate-and-fire model which is an idealization of a neuron with Ohmic leakage current [38], is computationally efficient and useful for analytical work. However, it is limited in generating rich spiking patterns. For instance, it does not have a spike generation mechanism for the regenerative upstroke of the membrane potential. Therefore, the Izhikevich model [39] is proposed to strike a tradeoff between the Hodgkin-Huxley model and the integrated-and-fire model, and inherits the merits of both models, namely biological plausibility and computational efficiency.

The Izhikevich model is given by

$$\frac{\mathrm{d}v}{\mathrm{d}t} = \alpha v^2 + \beta v + \gamma - u + I \tag{1}$$

$$\frac{\mathrm{d}u}{\mathrm{d}t} = a(bv - u), \tag{2}$$

where v denotes the membrane potential of a neuron, and u is the membrane recovery variable. α, β, γ, a, and b are parameters, and I is the input current. Whenever the membrane potential v is driven to some specific threshold $v_{\mathrm{T}} = 30\,\mathrm{mV}$, a spike is produced and the after-spiking resetting is triggered which is given by

$$\text{if } v \geq v_{\mathrm{T}}, \quad \text{then} \begin{cases} v \leftarrow c \\ u \leftarrow u + d. \end{cases} \tag{3}$$

The values of α, β, and γ in equation (1) are the same for all Izhikevich neurons. In contrast, the values of a, b in equations (2) and c, d in equation (3) vary according to the type of Izhikevich neurons. In this paper, we choose the values for the most typical Izhikevich neurons, namely regular spiking neurons [39]. The parameter values for the Izhikevich neuron model used in this paper are shown in Table 2.

Table 2. Parameter values for the Izhikevich neuron model.

	α	β	γ	a	b	c	d
value	0.04	5	140	0.02	0.2	-65	8
unit	$s^{-1}V^{-1}$	s^{-1}	Vs^{-1}	s^{-1}	N.A.	mV	mV

4.3. Spike train decoding schemes

Two spike train decoding schemes are evaluated in this paper: spike feature based *k*-nearest neighbors (SF-*k*NN) and spike train distance based *k*-nearest neighbors (STD-*k*NN).

4.3.1. Spike feature. It is generally considered that a majority of sensory neurons convey information by firing rate (FR), which refers to a temporal average [35]. The inverse of average interspike interval (ISI) is closely related to firing rate. It only considers the period between the first spike time and the last spike time. Another spike feature of equal importance is first spike latency. The tactile information of surface shape manipulated by the finger is found to be more reliably conveyed by the relative timing of the first spike latencies (FSL) [40].. In this work, both the firing rate and the inverse of average ISI are evaluated. The first spike latency is unconsidered in this paper because it is difficult to determine due to the operation of manual sliding.

4.3.2. Spike train distance. In this section, a wide variety of methods to quantify the similarity for spike trains are reviewed. Throughout the paper the following notation is used. The *i*-th spike train is denoted by $\mathbf{s}^i = \left\{t_1^i, t_2^i, \cdots, t_{N_i}^i\right\}$. N_i represents the total spike number. $t_j^i \ (j = 1, \cdots, N_i)$ is the *j*-th spike time of the *i*-th spike train.

The Victor-Purpura Distance: The Victor-Purpura distance [41] between two spike trains is defined as the minimum cost of carrying out a transformation of one spike train into the other. The distance calculation is performed through three elementary operations, which consists of spike deletion, spike insertion, and spike shift. Each operation is associated with an operation cost. Specifically, the operation of deleting a spike or inserting a spike is assigned a cost of one, while the cost of spike shift is set to $q|\Delta t|$, where $|\Delta t|$ is the temporal distance, and q is a spike timing-sensitive parameter.

The van Rossum Distance: For the van Rossum distance [42], spike train is first converted to continuous function by associating each spike with an exponential function. Given a spike train $\mathbf{s}=\{t_1, t_2,\cdots, t_N\}$, the resulting continuous function is defined as

$$f(t;\mathbf{s})=\sum_{i=1}^{N} H(t-t_i)e^{-(t-t_i)/\tau}, \tag{4}$$

where $H(t)$ is the Heaviside step function, and τ is the time constant. It is worth noting that the associated function could be functions other than the exponential. The van Rossum distance between two spike trains *m* and *n* is defined as the L_2 distance of the filtered spike trains, which is given by

$$D_{\mathrm{R}}(\mathbf{s}^m,\mathbf{s}^n)=\frac{1}{\tau}\int\left[f(t;\mathbf{s}^m)-f(t;\mathbf{s}^n)\right]^2 \mathrm{d}t. \tag{5}$$

The ISI Distance: In a comparison with the previous distances, the ISI distance [43] is parameter free, and is calculated on the basis of the instantaneous interspike interval, which is defined as

$$ISI(t)=t_{\mathrm{P}}(t)-t_{\mathrm{F}}(t), \tag{6}$$

where $t_{\mathrm{P}}(t)=\min(t_i|t_i>t)$ is the time of the preceding spikes and $t_{\mathrm{F}}(t)=\max(t_i|t_i<t)$ is the time of the following spikes. The resulting ratio function between the spike train *m* and *n* is given by

$$I(t)=\begin{cases}\dfrac{ISI^m(t)}{ISI^n(t)}-1 & \text{if } ISI^m(t)\le ISI^n(t)\\ 1-\dfrac{ISI^n(t)}{ISI^m(t)} & \text{otherwise.}\end{cases} \tag{7}$$

The ISI distance is derived by integrating $I(t)$ over time.

$$D_{\mathrm{ISI}}=\int |I(t)|\,\mathrm{d}t. \tag{8}$$

The SPIKE Distance: The SPIKE distance [44] is sensitive to spike coincidences and quantifies the similarity mediated by differences in spike timing. Suppose there are two spike trains *m* and *n*, the instantaneous difference of the preceding spikes is defined as

$$\Delta t_{\mathrm{P}}(t)=t_{\mathrm{P}}^m(t)-t_{\mathrm{P}}^n(t). \tag{9}$$

Similarly, we can obtain the instantaneous difference of the following spike $\Delta t_{\mathrm{F}}(t)=t_{\mathrm{F}}^m(t)-t_{\mathrm{F}}^n(t)$. The weighted average of the instantaneous spike difference is defined as

$$S(t)=\frac{|\Delta t_{\mathrm{P}}(t)|\langle w_{\mathrm{F}}(t)\rangle+|\Delta t_{\mathrm{F}}(t)|\langle w_{\mathrm{P}}(t)\rangle}{\langle ISI(t)\rangle^2}, \tag{10}$$

where the weights are given by $w_{\mathrm{P}}(t)=t-t_{\mathrm{P}}(t)$ and $w_{\mathrm{F}}(t)=t_{\mathrm{F}}(t)-\mathrm{t}$. $\langle\bullet\rangle$ denotes the average over spike trains. The SPIKE distance is then derived by integrating $S(t)$ over time

$$D_{\mathrm{SPIKE}}=\int S(t)\,\mathrm{d}t. \tag{11}$$

The Event-Synchronization Distance: The Event-Synchronization distance [45] is based on the relative timings of events. In this paper, the event is defined as spikes in the spike trains. The spikes t_i and t_j in the distinct spike trains, are assumed to be synchronous if the time difference is smaller than a time lag τ_{ij}, which is given by

$$\tau_{ij} = \min\left\{t_{i+1} - t_i, t_i - t_{i-1}, t_{j+1} - t_j, t_j - t_{j-1}\right\}/2 . \tag{12}$$

The number of times a spike appears in the spike train *m* shortly after a spike appears in spike train *n* is denoted by

$$c(m|n) = \sum_{i=1}^{N_m}\sum_{j=1}^{N_n} J_{ij} , \tag{13}$$

where J_{ij} is given by $J_{ij} = \begin{cases} 1 & \text{if } 0 < t_i^m - t_j^n \le \tau_{ij} \\ 1/2 & \text{if } t_i^m = t_j^n \\ 0 & \text{otherwise.} \end{cases}$

Similarly, we can define $c(n|m)$. The Event-Synchronization distance is computed as

$$D_{\text{Event-Syn}} = 1 - \frac{c(m|n) + c(n|m)}{\sqrt{N_m N_n}}. \tag{14}$$

4.3.3. k-nearest neighbors (kNN). *k*-nearest neighbors is a non-parametric classifier. The class of a test sample is determined by taking a majority vote of class labels among the *k* closest training samples. There are a variety of metrics to compute the distance between samples such as Euclidean distance (L_2 distance), L_1 distance and cosine distance. In this paper, the Euclidean distance is employed together with spike feature for SF-*k*NN, while the spike train distance is used for STD-*k*NN in spike train space. The choice of the value of *k* is crucial because a small *k* may lead to a classifier sensitive to noise samples, and a large *k* could result in less distinct boundaries between classes. The spike train distance based *k*-nearest neighbors algorithm is outlined in Figure 3.

Algorithm 1. Spike Train Distance based *k*NN (STD-*k*NN)

1: **Input:**
- Training set $\boldsymbol{S} = \{(\mathbf{s}^1, y^1), (\mathbf{s}^2, y^2), \cdots (\mathbf{s}^N, y^N)\}$, where $\mathbf{s}^i (i = 1, \cdots, N)$ is the spike train and $y^i \in (1, \cdots, C)$ is the associated class label
- Test sample $\mathbf{t}$

2: **for** $i = 1, \cdots, N$ **do**

3: Compute the spike train distance $D(\mathbf{s}^i, \mathbf{t})$

4: **end for**

5: Obtain the set $\boldsymbol{S}'$ of k closest training samples to $\mathbf{t}$

6: **Output:**

$y^* = \arg\max_{y'} \sum_{(\mathbf{s}^i, y^i) \in \boldsymbol{S}'} I(y^i = y')$, where $I(\cdot)$ is the indicator function

Figure 3. Spike train distance based *k*-nearest neighbors (STD-*k*NN) algorithm.

4.4. Experimental setup and protocol

The PVDF film sensor signals were amplified by a custom-built amplifier, and digitalized at a sampling rate of 1 kHz via an analog-to-digital converter (DAQCard USB-6225, National Instruments, USA). Supporting software was developed to record digital signals (LabVIEW, National Instruments, USA). Eight solid nickel test surfaces (Rubert & Co. Ltd., UK) with roughness values Ra of 50 μm (S1：

Surface 1), 25 µm (S2: Surface 2), 12.5 µm (S3: Surface 3), 6.3 µm (S4: Surface 4), 3.2 µm (S5: Surface 5), 1.6 µm (S6: Surface 6), 0.8 µm (S7: Surface 7), 0.4 µm (S8: Surface 8) were explored (Figure 4). The test surface finish was carried out using cylindrical turning.

Experimental neuroscientists have identified lateral sliding movements play a vital role in mediating surface roughness recognition [16]. The cutaneous vibrations generated during the lateral sliding are encoded by the fast adapting mechanoreceptors. In this paper, we manually performed this simple sliding movement to explore the surface roughness (Figure 4(b)). This movement has been used for object identification as well with precise motion control [46,47]. During the experiments, the sliding direction, speed and contact pressure were roughly controlled by the operator without relying on any motorized system. One PVDF film sensor was purposely put perpendicular to the sliding direction and denoted by PVDF film 1 while the other PVDF film sensor parallel to the sliding direction was denoted by PVDF film 2 (Figure 4(b)). The lateral sliding direction of the artificial fingertip along the test surface during our experiments is indicated by an arrow in Figure 4. Ten lateral sliding movements were performed on the eight test surfaces, resulting in 80 tactile time series samples. The sliding speed in our experiments was around 0.24 m/s. We also observed that that the magnitude of the signals will be smaller if the sliding speed is lower because the frequency of vibration is smaller when the sliding speed is lower. The sliding speed consistency and surface classification accuracy could be easily improved at the cost of including a speed controller.

The sensor outputs $V(t)$ were tuned with the electrical conductance G prior to analog-to-spike conversion. Specifically, the input current of the Izhikevich neuron model was obtained through the equation $I(t) = GV(t)$. The sample tactile signals generated by PVDF films and the corresponding spike trains transformed by spiking neuron models (i.e., the Izhikevich model) with the electrical conductance $G = 0.4\,\Omega^{-1}$ are shown in Figure 5. The effect of how to regulate the input current $I(t)$ by change the value of the electrical conductance is discussed in Section 5.

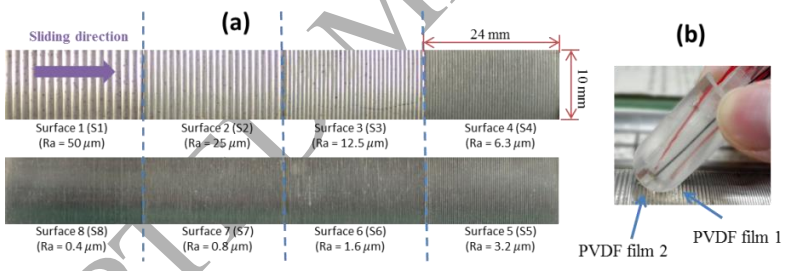

Figure 4. (a) Eight solid nickel standard surfaces with roughness values Ra of 50 µm, 25 µm, 12.5 µm, 6.3 µm, 3.2 µm, 1.6 µm, 0.8 µm, and 0.4 µm are explored. The lateral sliding direction of the artificial fingertip along the test surface during the conducted experiments is indicated by an arrow. (b) The locations of PVDF film sensors are indicated.

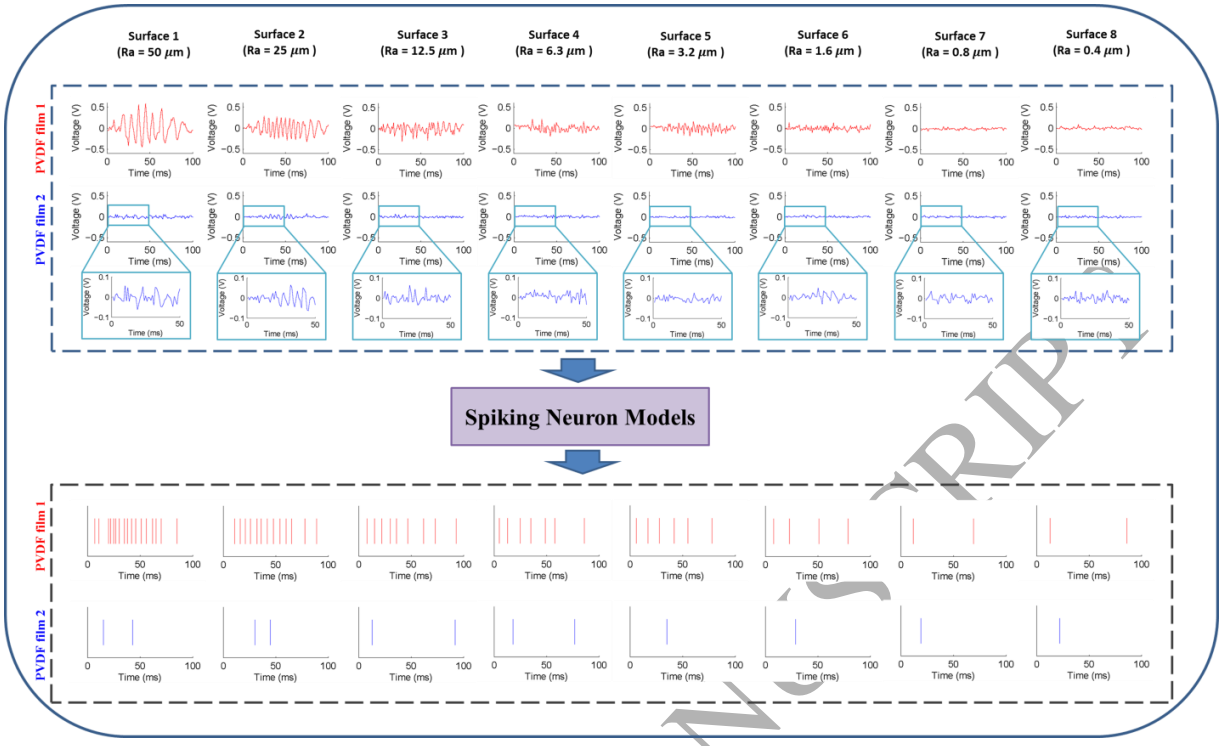

Figure 5. Typical tactile signals (top) generated by two PVDF films when laterally sliding on eight test surfaces with various roughness values, and the corresponding spike trains transformed via the Izhikevich model with electrical conductance $G = 0.4\ \Omega^{-1}$ (bottom).

5. Results and discussion

For each test surface, ten tactile time series samples were randomly split into the training set and the test set. This split procedure was repeated 500 times with ratios of 5:5, 7:3 and 9:1 between the training set and the test set. Table 3 shows that the highest classification accuracy based on different distributions between the training set and the test set. The highest classification accuracy is achieved with the ratio of 9:1, i.e., overfitting is not a problem with ratio of 9:1. In addition, the same split procedure was used in tactile object recognition [47]. The ratio between the training set and the test set is fixed to 9:1 in the following discussion.

Table 3. The highest classification accuracy based on various distributions between the training set and the test set.

Ratio Between the Training Set and the Test Set	*k* Value	Decoding Scheme	Best Classification Accuracy
5 : 5	7	*k*NN based on the Victor-Purpura distance	(72.3 ± 5.3)%
7 : 3	11	*k*NN based on the Victor-Purpura distance	(75.1 ± 6.5)%
9 : 1	11	*k*NN based on the Victor-Purpura distance	(77.6 ± 13.7)%

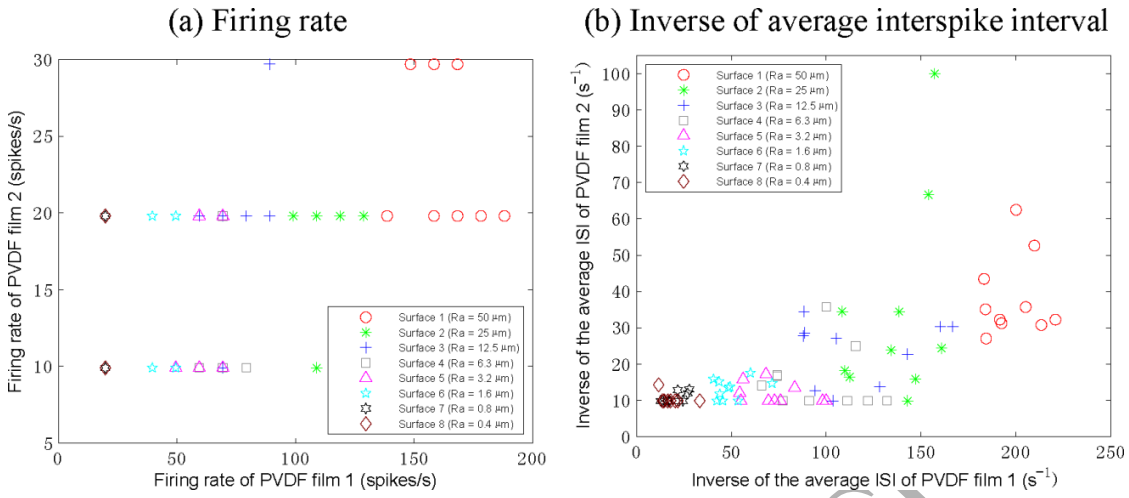

Figure 6. Spike features of two PVDF film sensors when laterally sliding on eight test surfaces with various roughness values. (a) Firing rate, (b) Inverse of average interspike interval.

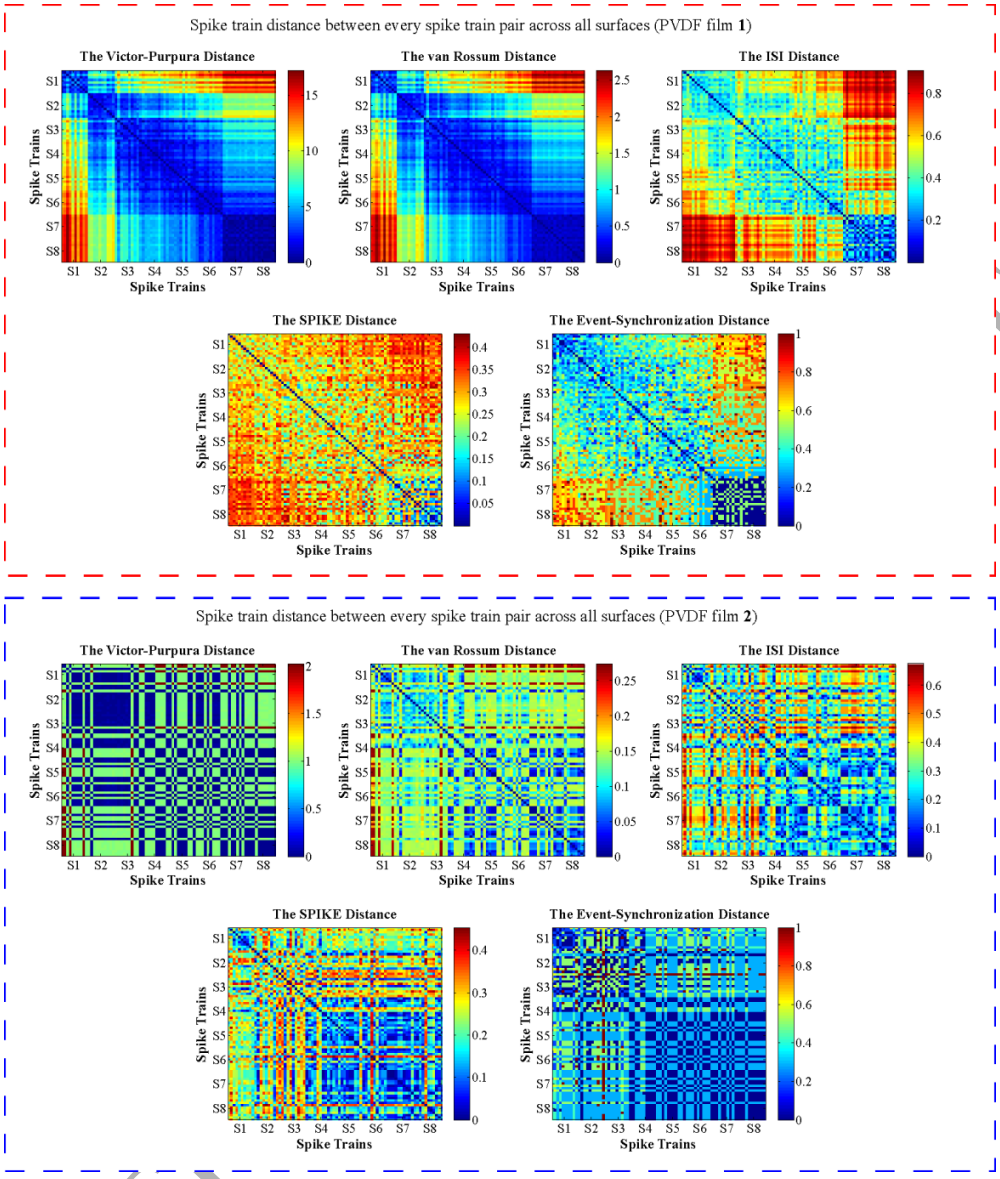

Figure 7. Different spike train distances between every spike train pair across eight test surfaces for both PVDF film1 (top) and PVDF film 2 (bottom).

Figure 6 shows the spike features of two PVDF film sensors when laterally sliding on eight test surfaces. Each point represents the result of one trial. It is shown that Surface 8 is distinguishable from other test surfaces for both firing rate and the inverse of average ISI. Surface 7 is more distinguishable for firing rate compared to average ISI. Firing rates of PVDF films, in particular for PVDF film 2 are completely overlapped for some trials, because the first spike time and the last spike time were not taken into account. Figure 7 depicts different spike train distances between every spike train pair across eight test surfaces for both PVDF films. It can be observed that the spike train distances between the pairs associated with the same test surface are much closer for both PVDF films. Ranges of all spike distances are much larger for PVDF film 1 compared to PVDF film 2.

The performances of spike train decoding schemes including SF-*k*NN and STD-*k*NN are evaluated. Classification accuracy of each decoding scheme for both PVDF film 1 (top) and PVDF film 2 (bottom) is compared (Figure 8). The highest classification accuracy using PVDF film 1 is (77.6 ± 13.7) % with

*k*NN (k = 11) classifier and the Victor-Purpura distance ($q = 0.024\ \mathrm{ms}^{-1}$). In contrast, PVDF film 2 possesses a much weak discriminative capability, and the best classification accuracy is (36.8 ± 13.0) % with *k*NN (k = 9) classifier and the van Rossum distance ($\tau = 96.81$ ms). As expected, the decoding schemes based on parameter-dependent spike train distances outperform the spike feature based decoding schemes, because parameter-dependent spike train distances take spike times into account and the parameters could be optimized for performance improvement. It is worth mentioning that a classification accuracy of (72.2 ± 10.9) % can be achieved by decoding scheme based on firing rate with *k*NN (k = 7) classifier, which means that the rate code might be accurate enough for roughness discrimination without taking the spike timing into further consideration.

The upper bound (red dash line in Figure 8) is the best classification result based on the analog signal without any analog-to-spike transformation, which can be found in our previous work [48]. The analog-to-spike conversion could be formulated as reduction of dimensionality [49]. Spike train has only one dimensional property, i.e., the spike time. The information loss arising from the transformation can be quantified by many measures such as information capacity and entropy [50]. For instance, Juusola and French [51] reported that the information capacity dropped from around 1400 bits/s (receptor current) to around 200 bits/s (action potentials), which provides a quantitative estimation of the cost of encoding analog signals into action potentials. In the context of the representation of surface roughness, it is shown (Figure 8) that the tactile information is mostly preserved, i.e., the transformation results in a decrease of the best classification accuracy by 5%.

Figure 9 shows the confusion matrix of the best classification results. The majority of misclassifications are between surface 7 (Ra = 0.8 μm) and surface 8 (Ra = 0.4 μm). In other words, the artificial fingertip is much more accurate to classify surfaces with roughness above 1 μm. If these two surfaces are eliminated from the examined set, the best classification accuracy of the remaining six surface classes increases to 83.4%. Furthermore, all the results in this paper have the same trend as those in our previous work based on analog signal processing [48].

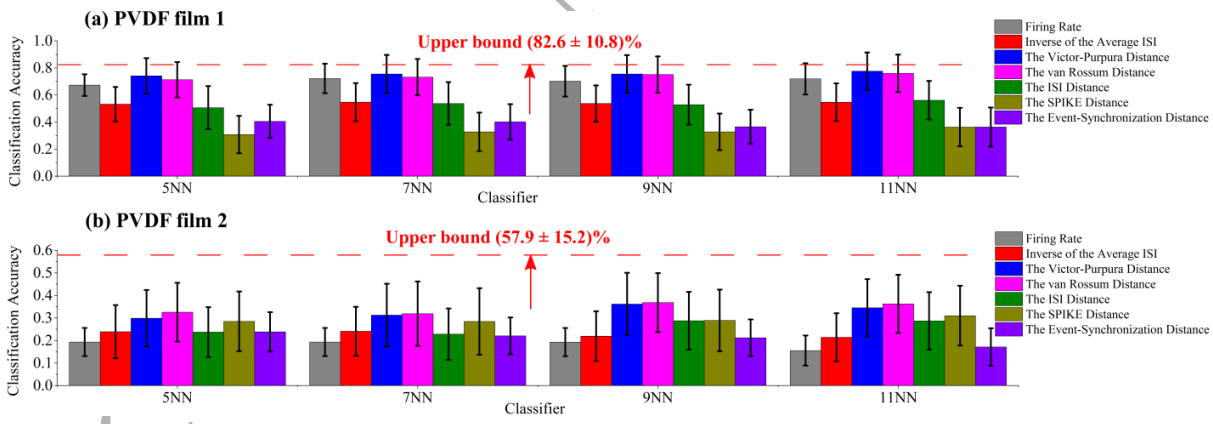

Figure 8. The classification accuracy of each decoding scheme is compared for both PVDF film 1 (top) and PVDF film 2 (bottom). The upper bound (red dash line) is the best classification result based on the analog signal without any analog-to-spike transformation in our previous work [48].

Classifier: *k*NN (k = 11) The Victor-Purpura Distance q = 0.024

	S1	S2	S3	S4	S5	S6	S7	S8	Accuracy
S1	500	0	0	0	0	0	0	0	100%
S2	0	494	6	0	0	0	0	0	98.8%
S3	0	0	338	114	48	0	0	0	84.5%
S4	0	0	50	317	133	0	0	0	63.4%
S5	0	0	0	92	387	21	0	0	77.4%
S6	0	0	0	0	34	466	0	0	93.2%
S7	0	0	0	0	0	0	258	242	51.6%
S8	0	0	0	0	0	0	154	346	69.2%

Overall Accuracy (Mean ± Standard deviation): (77.6 ± 13.7)%

Figure 9. Confusion matrix of the best classification result of the decoding schemes with *k*NN (k = 11) classifier and the Victor-Purpura distance ($q = 0.024\ \mathrm{ms}^{-1}$). The horizontal axis (S1-S8) denotes the ground truth, and the vertical axis represents the classifier output. The far right column presents the classification accuracy for each surface class.

Both the Victor-Purpura distance and the van Rossum distance are parameter-dependent. We investigate the classification accuracy using both spike train distances with respect to the associated parameters and Figure 10 depicts the evaluation of classification accuracy for PVDF film 1 with both parameter-dependent spike train distances for the value of k = 11. For the other values of k = 5, 7, 9, the recognition performances as a function of the associated parameters have the similar trend.

The electrical conductance can regulate the input current of the Izhikevich model and eventually influence the classification accuracy. We tune the electrical conductance and evaluate the performance of classifiers based on the Victor-Purpura distance and the van Rossum distance. It is shown (Figure 11) that the highest classification accuracy is (77.6 ± 13.7) % with the Victor-Purpura distance (G = 0.4 Ω^{-1}) for PVDF film 1 and (47.5 ± 16.2) % with the Victor-Purpura distsance (G = 1.4 Ω^{-1}) for PVDF film 2.

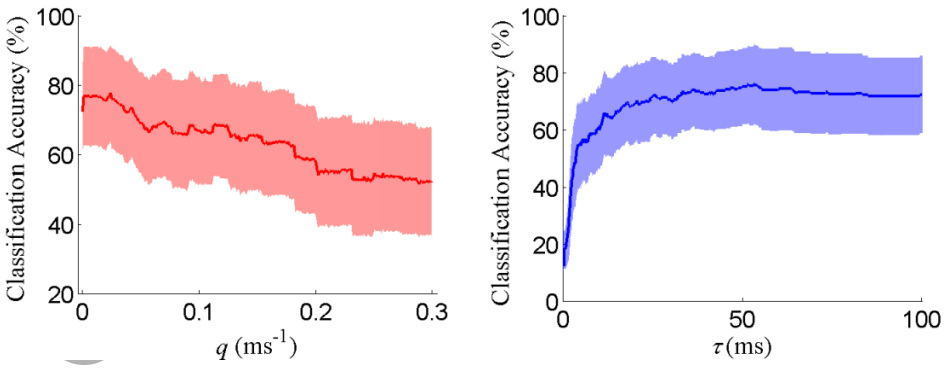

Figure 10. Evaluation of classification accuracy of STD-*k*NN (the Victor-Purpura distance and k = 11) with respect to the spike timing-sensitive parameter q for PVDF film 1 (left). Evaluation of classification accuracy of STD-*k*NN (the van Rossum distance and k = 11) with respect to the time constant τ for PVDF film 1 (right).

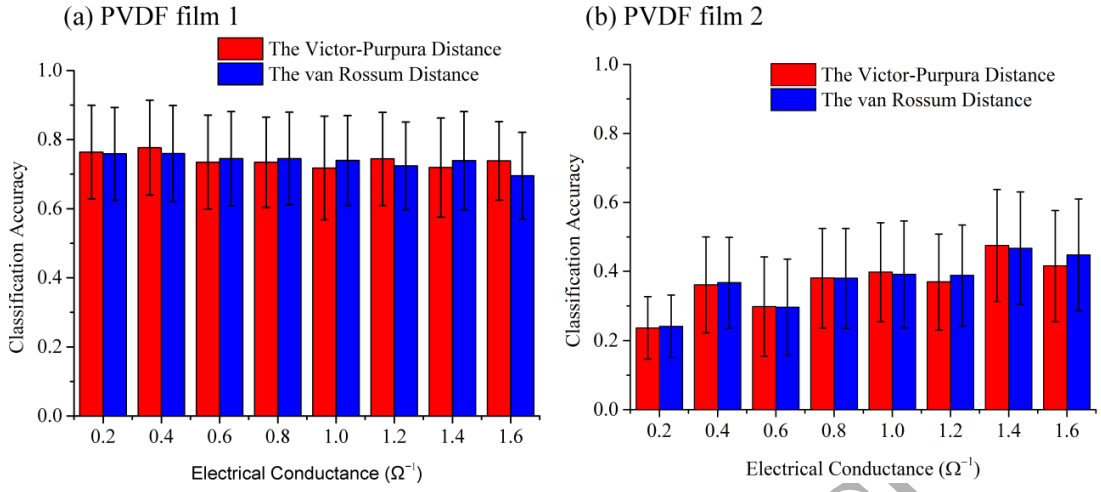

Figure 11. Evaluation of classification accuracy of STD-*k*NN (the Victor-Purpura distance and the van Rossum distance) with respect to the electrical conductance *G*. (a) PVDF film 1, (b) PVDF film 2.

The presented work can be extended in several directions that might improve the classification accuracy. One direction is to improve the hardware. For instance, more PVDF films could be integrated in the biomimetic fingertip in order to obtain more information. The investigation of how the positions of sensing elements affect the performance would be interesting as well. Another direction focuses on the signal processing level. The spike trains from multiple sensors form a spike network. Therefore, supervised learning algorithms such as Tempotron [26] could be employed to fuse the spike trains.

6. Conclusion

We have presented a soft neuromorphic approach for performing tactile surface roughness discrimination with a biologically inspired artificial fingertip. The Ra value range of test surfaces is from 0.4 µm to 50 µm. Five spike train distances and spike features together with the *k*NN classifiers were used and the best classification accuracy is (77.6 ± 13.7) % obtained using *k*NN (k = 11) classifier and the Victor-Purpura distance ($q = 0.024\ \mathrm{ms}^{-1}$). The best classification accuracy decreases by only 5% compared to the analog tactile signal interpretation in our previous work, which indicated that the tactile information is mostly preserved in the context of surface roughness representation during the analog-to-spike transformation. All the experimental data were collected by manually sliding the artificial fingertip on the testing surfaces without using any controller for either sliding speed or normal load, i.e., the developed approach is very robust and suitable for real time surface roughness evaluation. The study of a soft neuromorphic approach for tactile surface roughness discrimination may provide new insight into the development of advanced neuroprostheses and neurorobots.

Acknowledgement

This project is supported by the Joint PhD Degree Programme NTU–TU Darmstadt. The project is also supported by Fraunhofer Singapore, which is funded by the National Research Foundation (NRF) and managed through the multi-agency Interactive & Digital Media Programme Office (IDMPO) hosted by the Infocomm Media Development Authority of Singapore (IMDA). YL Zhang acknowledges the financial support of this research by the A*STAR AOP project (1223600005) and the A*STAR Industrial Robotics Programme (1225100007). The authors would like to thank Dr. Thomas Kreuz for the helpful discussion on spike train distance and the anonymous reviewers for their constructive comments.

References

[1] S.C. Liu, T. Delbruck, Neuromorphic sensory systems, Curr. Opin. Neurobiol. 20 (2010) 288–295.

[2] K.A. Boahen, Point-to-point connectivity between neuromorphic chips using address events, IEEE Trans. Circuits Syst. II Analog Digit. Signal Process. 47 (2000) 416–434.
[3] A.Y. Chow, The Artificial Silicon Retina Microchip for the Treatment of VisionLoss From Retinitis Pigmentosa, Arch. Ophthalmol. 122 (2004) 460.
[4] T.J. Hamilton, C. Jin, A. van Schaik, J. Tapson, An active 2-D silicon cochlea, IEEE Trans. Biomed. Circuits Syst. 2 (2008) 30–43.
[5] G. Spigler, C.M. Oddo, M.C. Carrozza, Soft-neuromorphic artificial touch for applications in neuro-robotics, 4th IEEE RAS EMBS Int. Conf. Biomed. Robot. Biomechatronics. (2012) 1913–1918.
[6] A. Roberts, B.M.H. Bush, Neurones without impulses: their significance for vertebrate and invertebrate nervous systems, Cambridge University Press, 1981.
[7] R.A. DiCaprio, C.P. Billimoria, B.C. Ludwar, Information rate and spike-timing precision of proprioceptive afferents., J. Neurophysiol. 98 (2007) 1706–1717.
[8] B. Sengupta, S.B. Laughlin, J.E. Niven, Consequences of Converting Graded to Action Potentials upon Neural Information Coding and Energy Efficiency, PLoS Comput. Biol. 10 (2014).
[9] T.R. Jack JJB, Noble D, Electric Current Flow in Excitable Cells, Clarendon Press. Oxford. (1975).
[10] S.B. Laughlin, R.R.D.R. Van Steveninck, J.C. Anderson, The metabolic cost of neural information, 1 (1998).
[11] W.W. Lee, H. Yu, N. V. Thakor, Gait event detection through neuromorphic spike sequence learning, in: 5th IEEE RAS/EMBS Int. Conf. Biomed. Robot. Biomechatronics, 2014: pp. 899–904.
[12] L.L. Bologna, J. Pinoteau, J.-B. Passot, J.A. Garrido, J. Vogel, E.R. Vidal, A. Arleo, A closed-loop neurobotic system for fine touch sensing, J. Neural Eng. 10 (2013) 46019.
[13] W. Tang, Y. Zhou, H. Zhu, H. Yang, The effect of surface texturing on reducing the friction and wear of steel under lubricated sliding contact, Appl. Surf. Sci. 273 (2013) 199–204.
[14] M.A.L. Nicolelis, M.A. Lebedev, Principles of neural ensemble physiology underlying the operation of brain-machine interfaces., Nat. Rev. Neurosci. 10 (2009) 530–40.
[15] L. Skedung, M. Arvidsson, J.Y. Chung, C.M. Stafford, B. Berglund, M.W. Rutland, Feeling small: exploring the tactile perception limits, Sci. Rep. 3 (2013).
[16] X. Libouton, O. Barbier, Y. Berger, L. Plaghki, J.-L. Thonnard, Tactile roughness discrimination of the finger pad relies primarily on vibration sensitive afferents not necessarily located in the hand, Behav. Brain Res. 229 (2012) 273–279.
[17] C.E. Connor, K.O. Johnson, Neural coding of tactile texture: comparison of spatial and temporal mechanisms for roughness perception, J. Neurosci. 12 (1992) 3414–3426.
[18] T. Yoshioka, B. Gibb, A.K. Dorsch, S.S. Hsiao, K.O. Johnson, Neural coding mechanisms underlying perceived roughness of finely textured surfaces, J. Neurosci. 21 (2001) 6905–6916.
[19] W.W. Mayol-Cuevas, J. Juarez-Guerero, S. Munoz-Gutierrez, A first approach to tactile texture recognition, IEEE Int. Conf. Syst. Man, Cybern. 5 (1998) 4246–4250.
[20] H.B. Muhammad, C. Recchiuto, C.M. Oddo, L. Beccai, C.J. Anthony, M.J. Adams, M.C. Carrozza, M.C.L. Ward, A capacitive tactile sensor array for surface texture discrimination, Microelectron. Eng. 88 (2011) 1811–1813.
[21] F. De Boissieu, C. Godin, B. Guilhamat, D. David, C. Serviere, D. Baudois, Tactile texture recognition with a 3-axial force MEMS integrated artificial finger, in: Robot. Sci. Syst., 2009.
[22] O. Kroemer, C.H. Lampert, J. Peters, Learning dynamic tactile sensing with robust vision-based training, IEEE Trans. Robot. 27 (2011) 545–557.
[23] C.M. Oddo, M. Controzzi, L. Beccai, C. Cipriani, M.C. Carrozza, Roughness encoding for discrimination of surfaces in artificial active-touch, IEEE Trans. Robot. 27 (2011) 522–533.
[24] E. Peiner, M. Balke, L. Doering, Slender tactile sensor for contour and roughness measurements within deep and narrow holes, IEEE Sens. J. 8 (2008) 1960–1967.
[25] W.W. Lee, J.-J. Cabibihan, N. V Thakor, Bio-mimetic strategies for tactile sensing, IEEE SENSORS. (2013) 1–4.

[26] R. Gütig, H. Sompolinsky, The tempotron: a neuron that learns spike timing–based decisions, Nat. Neurosci. 9 (2006) 420–428.
[27] U.B. Rongala, A. Mazzoni, C.M. Oddo, Neuromorphic Artificial Touch for Categorization of Naturalistic Textures, IEEE Trans. Neural Networks Learn. Syst. (2015).
[28] S. Najarian, J. Dargahi, A.A. Mehrizi, Artificial tactile sensing in biomedical engineering, 1st ed., McGraw-Hill Education, New York, 2009.
[29] G.J. Augustine, D.M. Chikaraishi, M.D. Ehlers, G. Einstein, D. Fitzpatrick, W.C. Hall, E. Jarvis, L.C. Katz, J. Kauer, A.-S. LaMantia, J.O. McNamara, R.D. Mooney, M.A.L. Nicolelis, D. Purves, P.H. Reinhart, S.A. Simon, J.H.P. Skene, J. Voyvodic, L.E. White, S.M. Williams, Neuroscience, 3rd ed., Sinauer Associates, Inc., Massachusetts, 2004.
[30] R.D. Howe, M.R. Cutkosky, Dynamic tactile sensing: Perception of fine surface features with stress rate sensing, IEEE Trans. Robot. Autom. 9 (1993) 140–151.
[31] B. Choi, H.R. Choi, S. Kang, Development of tactile sensor for detecting contact force and slip, IEEE/RSJ Int. Conf. Intell. Robot. Syst. (2005) 2638–2643.
[32] S. Sokhanvar, M. Packirisamy, J. Dargahi, A multifunctional PVDF-based tactile sensor for minimally invasive surgery, Smart Mater. Struct. 16 (2007) 989.
[33] A. Kimoto, N. Sugitani, S. Fujisaki, A multifunctional tactile sensor based on PVDF films for identification of materials, IEEE Sens. J. 10 (2010) 1508–1513.
[34] Z. Yi, Y. Zhang, Bio-inspired Tactile FA-I Spiking Generation under Sinusoidal Stimuli, J. Bionic Eng. 13 (2016) 612–621.
[35] W. Gerstner, W.M. Kistler, Spiking neuron models: Single neurons, populations, plasticity, Cambridge university press, 2002.
[36] A.L. Hodgkin, A.F. Huxley, A quantitative description of membrane current and its application to conduction and excitation in nerve, J. Physiol. 117 (1952) 500.
[37] R.B. Stein, Some Models of Neuronal Variability, Biophys. J. 7 (1967) 37–68.
[38] E.M. Izhikevich, Dynamical systems in neuroscience, 1st ed., The MIT press, London, 2007.
[39] E.M. Izhikevich, Simple model of spiking neurons, IEEE Trans. Neural Networks. 14 (2003) 1569–1572.
[40] R.S. Johansson, I. Birznieks, First spikes in ensembles of human tactile afferents code complex spatial fingertip events, Nat. Neurosci. 7 (2004) 170–177.
[41] J.D. Victor, K.P. Purpura, Nature and precision of temporal coding in visual cortex: a metric-space analysis, J. Neurophysiol. 76 (1996) 1310–1326.
[42] M.C.W. van Rossum, A novel spike distance, Neural Comput. 13 (2001) 751–763.
[43] T. Kreuz, J.S. Haas, A. Morelli, H.D.I. Abarbanel, A. Politi, Measuring spike train synchrony, J. Neurosci. Methods. 165 (2007) 151–161.
[44] T. Kreuz, D. Chicharro, M. Greschner, R.G. Andrzejak, Time-resolved and time-scale adaptive measures of spike train synchrony, J. Neurosci. Methods. 195 (2011) 92–106.
[45] R. Quian Quiroga, T. Kreuz, P. Grassberger, Event synchronization: A simple and fast method to measure synchronicity and time delay patterns, Phys. Rev. E. 66 (2002) 41904.
[46] J. Edwards, J. Lawry, J. Rossiter, C. Melhuish, Extracting textural features from tactile sensors, Bioinspir. Biomim. 3 (2008) 35002.
[47] J. Hoelscher, J. Peters, T. Hermans, Evaluation of tactile feature extraction for interactive object recognition, in: IEEE-RAS 15th Int. Conf. Humanoid Robot., 2015: pp. 310–317.
[48] Z. Yi, Y. Zhang, J. Peters, Bioinspired tactile sensor for surface roughness (accepted), Sensors Actuators, A Phys.
[49] B.A. y Arcas, A.L. Fairhall, W. Bialek, Computation in a Single Neuron: Hodgkin and Huxley Revisited, Neural Comput. 15 (2003) 1715–1749.
[50] A.S. French, K. Pfeiffer, Measuring entropy in continuous and digitally filtered neural signals, J. Neurosci. Methods. 196 (2011) 81–87.
[51] M. Juusola, A.S. French, The efficiency of sensory information coding by mechanoreceptor neurons, Neuron. 18 (1997) 959–968.

Zhengkun Yi received his B.S. degree from University of Science and Technology of China (USTC) and M.E. degree from Chinese Academy of Sciences (CAS). He is currently a PhD student in the joint PhD degree programme between Nanyang Technological University (NTU) and Technische Universitaet Darmstadt (TUDa). His research interests include biomimetic tactile sensing and exploration, sensor fabrication technologies, machine learning, and computational neuroscience.

Yilei Zhang received his Ph.D degree (2007) from Iowa State University in mechanical engineering and electrical engineering. Before joining Nanyang Technological University in 2012, he served as a senior research engineer in the Goodyear Tire and Rubber Company. His research interests include neuroengineering, bioinspired sensors, etc.